

VIBRATION MEASUREMENT FOR CRACK AND RUB DETECTION IN ROTORS

Ali Hajnayeb, Kourosh Heidari Shirazi, Reza Aghamiri

Shahid Chamran University of Ahvaz, Faculty of Engineering Ahvaz, Daneshgah Square, Iran (✉ a.nayeb@scu.ac.ir, +98 912 516 2248, k.shirazi@scu.ac.ir, rezaaghamiri1@gmail.com)

Abstract

Shaft-stator rub and cracks on rotors, which have devastating effects on the industrial equipment, cause non-linear and in some cases chaotic lateral vibrations. On the other hand, vibrations caused by machinery faults can be torsional in cases such as rub. Therefore, a combined analysis of lateral and torsional vibrations and extraction of chaotic features from these vibrations is an effective approach for rotor vibration monitoring. In this study, lateral and torsional vibrations of rotors have been examined for detecting cracks and rub. For this purpose, by preparing a laboratory model, the lateral vibrations of a system with crack and rub have been acquired. After that, a practical method for measuring the torsional vibrations of the system is introduced. By designing and installing this measurement system, practical test data were acquired on the laboratory setup. Then, the method of phase space reconstruction was used to examine the effect of faults on the chaotic behaviour of the system. In order to diagnose the faults based on the chaotic behaviour of the system, *largest Lyapunov exponent* (LLE), *approximate entropy* (ApEn) and correlation dimension were calculated for a healthy system and also for a system with rub and a crack. Finally, by applying these parameters, the chaotic feature space is introduced in order to diagnose the intentionally created faults. The results show that in this space, the distinction between the various defects in the system can be clearly identified, which enables to use this method in fault diagnosis of rotating machinery.

Keywords: rotor vibrations, crack, rub, fault detection, chaos features, largest Lyapunov exponent, approximate entropy, correlation dimension.

© 2020 Polish Academy of Sciences. All rights reserved

1. Introduction

Rotors are one of the most critical parts in almost all types of rotating machinery. Normally, they transfer the generated torque from a driver to a driven machine. Most of the industrial rotors are heavy and rotate at high speeds that store significant kinetic energy in them. Any fault or disturbance in normal operation of the system can release a part or all of this energy and results in a catastrophic event. One of the common faults in rotors is crack. Cracks grow gradually and result in a sudden fracture of a rotor. Another common fault in rotors is the occurrence of rub between stators and rotors or any rotating part, which is installed on it (*e.g.* blades). It can be caused by bending, misalignment, unbalance, poor lubrication, *etc.* To protect rotors from failures

initiated by faults like crack and rub, several fault detection and diagnosis techniques have been proposed.

Although the symptoms of faults can be observed through applying many vibration analysis techniques such as spectrum analysis, wavelet analysis, order tracking *etc.* [1, 12, 24], a large number of studies have been carried out based on the extraction of a series of features from vibration signals and applying artificial intelligence to fault diagnosis [2, 3, 5]. Commonly, time, frequency or time-frequency domain features are extracted from a machinery vibration signal. These techniques and features are effective for simple systems and faults. More complex systems and faults that show nonlinear or chaotic behaviour need applying innovative processing techniques and vibration features. The theoretical model and practical analysis of a number of faults demonstrate nonlinear or chaotic behaviour [7, 8, 11]. Therefore, chaotic parameters have been used in rotating machinery as diagnosis tools, recently.

One of the informative chaotic parameters is the “correlation dimension”. Wang *et al.* [21] used correlation dimension in detecting rub between a rotor and its stator. They ameliorated the G-P algorithm, which had been used for calculating correlation dimension. They also decreased the computation time by proposing a new method for computing distances between vectors. In another study, Wang *et al.* [22] examined the simultaneous use of correlation dimension and spectrum analysis in fault diagnosis of rotating machinery. They studied the feasibility of applying chaotic parameters in intelligent diagnosis systems. Zhihong and Yongqiang [25] used nonlinear dynamics for fault diagnosis of a wheelset bearing. In addition to the correlation dimension, they used a method of phase space reconstruction to diagnose different fault conditions. The correlation dimension showed more promising results. Shuting *et al.* [16] proposed a method for fault diagnosis of a turbine-generator based on correlation dimension and *artificial neural network* (ANN). They found that the vibration spectra in healthy and faulty conditions are almost the same, while the values of correlation dimension are different in the three fault conditions. Therefore, they used it as the input to an ANN. Correlation dimension is not the only feature used in this field and there are similar features as well.

Another common chaotic parameter that has been used in vibration-based diagnosis is ApEn of the signal. Yan and Gao [23] examined the feasibility of applying ApEn in condition monitoring of machinery. They tried to find a quantitative tool for evaluating the relation between the signal complexity (defined as the number of its frequency components and its noise level) and the change in the value of entropy. In their research, they studied the effect of dimension, tolerance and data length on the value of entropy and the diagnosis results. He and Zhang [6] used ApEn in fault diagnosis of rolling element bearings and studied its sensitivity to the fault condition. They implemented their method on both simulation and test signals. The effects of working conditions such as radial load, speed and fault level on the value of ApEn of a vibration signal were also examined. In a similar study, Zhou *et al.* [26] and Sadooghi and Kadem [15] used nonlinear features including ApEn for health assessment of roller bearings.

The next parameter in this field is Lyapunov exponent. Wang *et al.* [20] applied it to fault diagnosis of roller bearings. They studied the change in the value of the largest Lyapunov exponent extracted from the vibration signal of a bearing in different fault conditions and found it sensitive to the faults. Lu *et al.* [9] also used Lyapunov exponent in addition to correlation dimension and ApEn to diagnose bearings. Soleimani and Khadem [17] extended these studies by applying chaotic parameters to fault diagnosis of a gearbox. They studied the change in the value of parameters for different fault conditions.

Most of the aforementioned research on crack and rub detection was based on the measurement of only the lateral vibrations of a rotor despite the fact that the torsional vibrations also include useful information. The torsional vibration measurement is helpful especially in detecting faults

such as rub that induce significant torsional vibrations. Vance and French [19] measured and analysed the torsional vibrations of several laboratory test setups. They proposed a method of “time of arrival” for torsional vibration measurement. Maynard and Trethewey [10] examined the feasibility of applying this method of torsional vibration measurement to crack detection in turbine blades. They tried to measure the change in the natural frequency of a blade caused by cracks in the blade through measuring the torsional vibrations of the rotor. Resor *et al.* [13] studied the effects of defects in the encoders and shaft speed variations on the measured torsional vibrations. They used an averaging method to compensate for the caused errors. Trethewey *et al.* [18] studied the impact of the type of encoder on the measured vibrations of a rotor. They proposed a minimally intrusive method in their research.

As discussed in this section, in most of the previous studies, vibration behaviour of a cracked rotor or a rotor with rub have been studied extensively, but separately. However, a crack in rotor usually results in more flexibility and higher vibration amplitudes. This increase in vibration amplitudes increases the probability of rub between rotor and stator and makes the fault diagnosis more complicated. In this research, the case of simultaneous occurrence of rub and crack in a rotor was examined, in addition to the separate cases of rub or crack. A laboratory test setup for simulating crack and rub was prepared. Lateral and torsional vibration signals of a rotor were recorded in normal conditions, rotor-stator rub, rotor crack and a condition of combined rub and crack. In order to detect these two faults, first the phase space of the system was reconstructed using the rotor vibration signals. Then, a number of chaotic features were extracted from the reconstructed phase space. After that, the values of the extracted features in each fault condition were plotted. The changes in the values of these features in faulty cases compared with those obtained in the normal condition are significant. The feature space was also plotted for the studied health conditions. The results show the effectiveness of the extracted features and also the potential use of torsional vibrations in crack and/or rub detection of rotors.

2. Theory

2.1. Phase space reconstruction

The state space of a dynamical system shows the behaviour and condition of that system. In machinery vibration monitoring, normally a one-dimensional time series is recorded by using only one type of sensor installed in each specific measurement point. Therefore, the time series has to be extended to a higher-dimensional phase space. It can be performed by using the theorem of embedding. This theory presents that the measurements of a state of a system have enough information on other states of the system. As a result, using an appropriate transformation the state space of the system can be reconstructed in a way that is based on the information of the original system. Based on Taken’s theorem, if a time series x_i of a dynamical system is available, where $i = 1, 2, \dots, N$ and N is the length of the time series, then the vector of the state space of the system can be constructed as:

$$Y_j = [x_j, x_{j+T}, x_{j+2T}, \dots, x_{j+(d-1)T}], \quad (1)$$

where:

$$j = 1, 2, \dots, N - (d - 1)T. \quad (2)$$

In (1) and (2), d is the embedding dimension and T is the time delay. In fact, the embedding dimension is the number of vectors in the matrix shown in (1), which is equal to the dimensions

of the reconstructed state space. The time delay is the time difference between two corresponding elements of these two vectors.

2.2. Determining embedding dimension and time delay

In order to find the values of embedding dimension and time delay, the fact is used that trajectories of a dynamical system do not intersect. Actually, embedding dimension is the minimum number of dimensions needed for reconstruction of the phase space in such a way that no intersection occurs in the extended phase space. One of the common methods for determining the embedding dimension is counting the false nearest neighbours. According to [20], here, the minimum value of the embedding dimension is considered as $d = 2$. The value of time delay has to be determined as well. The method of average mutual information is used in the current study to find the best value for time delay. The mutual information between x_i and x_{i+T} is defined as [20]:

$$I(T) = \sum_i P[x_i, x_{i+T}] \log_2 \left[\frac{P[x_i, x_{i+T}]}{P[x_i]P[x_{i+T}]} \right], \quad (3)$$

where $I(T)$, x_i and x_{i+T} are the average mutual information function, the original time series and the delayed time series, respectively. $P[x_i]$ and $P[x_{i+T}]$ are the probabilities of occurrence of x_i and x_{i+T} , respectively. $P[x_i, x_{i+T}]$ is the joint probability of occurrence of x_i and x_{i+T} . The value of T at which the first minimum of $I(T)$ function is observed is considered as the optimum delay time.

2.3. Chaotic features

2.3.1. Largest Lyapunov exponent

Lyapunov exponent is a parameter that characterizes the rate of separation of two close trajectories in the phase space of a system. Rosenstein *et al.* [25] proposed an expression for calculating the *largest Lyapunov exponent* (LLE) of a time series as:

$$\lambda_1 = \frac{1}{\Delta t \times M} \sum_{j=1}^M \ln \frac{L(t_j)}{L(t_{j-1})}, \quad (4)$$

where Δt and L are the sampling time and the minimum distance between two points of the time series, respectively. M is the number of reconstructed points and is defined as:

$$M = N - (d - 1)T. \quad (5)$$

2.3.2. Correlation dimension

Correlation dimension is an index of complexity of a dynamical system and can be used to detect chaotic behaviour. It is calculated by using a correlation integral function, $C(r, N)$, which is defined as the ratio of the number of close points in the sphere of radius r to the total number of points (N). From all the available algorithms for calculating the correlation function, Grassberger-Procaccia's algorithm is applied more often than others [26]. In this algorithm, a set of points $\{X_i, i = 1, 2, \dots, N$ is considered on the attractor, and the correlation function is

defined as:

$$C(r) = \lim_{N \rightarrow \infty} \frac{2}{N^2} \sum_{\substack{i,j=1 \\ i \neq j}}^N H(r - [X_i - X_j]), \quad (6)$$

where r is the radius of a sphere with X_i or X_j as its centre. X_i is a point on the attractor and the Heaviside function $H(r - [X_i - X_j])$ checks its distance to X_j , and if it is located in the sphere, adds it to the other points used in calculating the correlation function. The correlation dimension, ν , for a specific embedding dimension is defined as:

$$\nu = \lim_{\substack{r \rightarrow 0 \\ N \rightarrow \infty}} \frac{\log C(r)}{\log r}. \quad (7)$$

2.3.3. Approximate entropy (ApEn)

ApEn is an approximation of the complexity of a time series and determines the degree of unpredictability of a signal. Low values of ApEn show that the time series is predictable and high values of ApEn mean the time series is unpredictable. The first step of calculating ApEn is defining a vector as:

$$X(i) = \{x(i), x(i + 1), x(i + 2), \dots, x(i + d - 1)\}, \quad i = 1, 2, \dots, N-d+1, \quad (8)$$

where d is the embedding dimension and N is the length of the time series. The distance between two vectors is defined as the maximum difference between its elements:

$$d[X(i), X(j)] = (|x(i + k - 1)| - |x(j + k - 1)|), \quad (9)$$

$$i = 1, 2, \dots, N-d+1, \quad j = 1, 2, \dots, N-d+1.$$

Now, $C_i^d(r)$ is defined as:

$$C_i^d(r) = \frac{1}{N - (d - 1)} \sum_{j \neq i} \Theta\{r - d[X(i), X(j)]\}, \quad j = 1, 2, \dots, N-d+1, \quad j \neq i, \quad (10)$$

where $\Theta\{x\}$ is a unit step function, and:

$$r = k \times std(X). \quad (11)$$

In (15), $std(X)$ is the standard deviation of X , and k is a constant. Then, $\phi^d(r)$ is defined as:

$$\phi^d(r) = \frac{1}{N - d + 1} \sum_{i=1}^{N-d+1} \ln [C_r^d(i)]. \quad (12)$$

Finally, the ApEn of a time series is defined as:

$$AE(d, r, N) = \phi^d(r) - \phi^{d+1}(r). \quad (13)$$

3. Laboratory setup

A series of laboratory tests were carried out on a rotor shown in Fig. 1 in order to evaluate the performance of the proposed approach. This system comprises two discs that are fixed to a shaft.

An electrical motor drives the shaft. In order to simulate a crack, a flange is placed in the middle of the shaft (the shaft has two parts that are attached through the flange). By removing a number of screws out of the six screws of the flange, a crack can be simulated (Fig. 2). Rotor-stator rub is simulated by attaching a hard plastic part to the flange and its collision with a rigid and fixed rod in each shaft rotation. By applying a radial force to point (6) of Fig. 1 using a belt under tension, the crack behaviour is obtained.

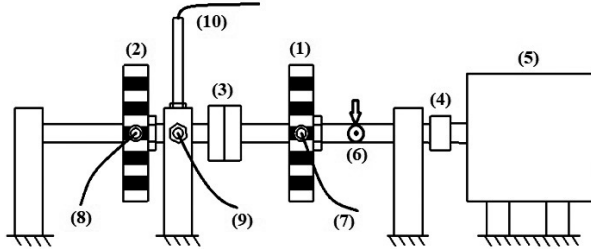


Fig. 1. A schematic view of the test setup: (1) and (2) discs; (3) flange; (4) coupling; (5) electrical motor; (6) radial force; (7) and (8) fiber-optic sensors; (9) and (10) displacement sensors.

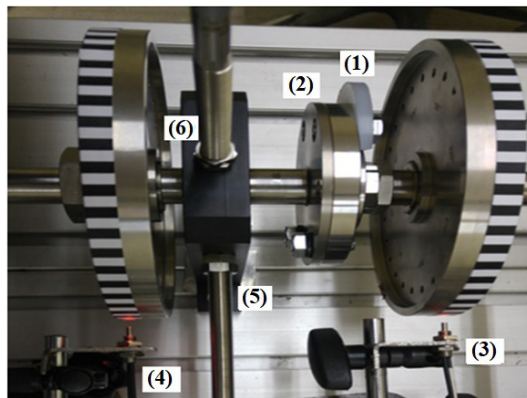


Fig. 2. A photo of the test setup: (1) hard plastic part for rub simulation; (2) flange; (3) and (4) fiber-optic sensors; (5) and (6) displacement sensors.

Lateral vibrations of the rotor are recorded by using two noncontact displacement sensors. The IN-085 B&K displacement sensors are installed to measure the horizontal and vertical vibrations of the rotor close to a simulated crack. The outputs of these sensors are provided into a conditioner and its output is acquired by the B&K Pulse data acquisition system. The torsional vibrations are also measured. For that purpose, two zebra tapes are attached to the two discs and one of OPTEX NF-DB01 fibre-optic sensors is installed in front of each tape. Each zebra tape has 50 white and 50 black lines. Optical fibre sensors send the corresponding pulse-train signals of the colour switching of the zebra tape to a Saleae 8ch – 24 MHz logic analyser. The analyser is connected to a computer and the pulse trains are recorded with a sampling rate of 2 MHz. A screen shot of the software of the analyser is shown in Fig. 3. The torsional vibration is extracted from the recorded pulse trains with the method discussed in the next section. The data are recorded at two different rotational speeds of 600 rpm and 1200 rpm. At each speed, the fully fastened flange and partially fastened flange (cracked rotor) are tested.

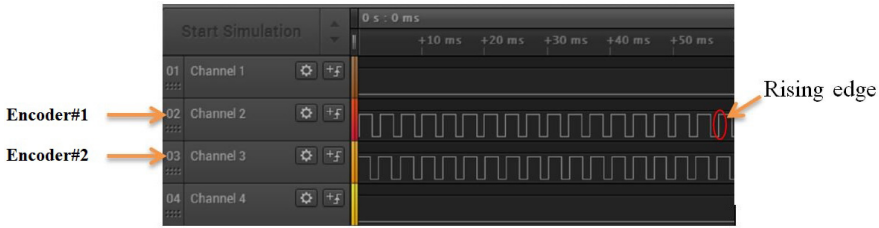


Fig. 3. Recorded signals of the encoders.

4. Torsional vibration measurement

In this study, the time of arrival is used to measure the torsional vibrations of the system. This method is based on measurement of the moments when the encoder divisions pass a specific location and comparing these moments with a reference signal. When the rotor is rotating with a constant speed and without torsional vibrations, theoretically the time intervals between passage times of the encoder divisions remain constant. In the case of torsional vibrations, speed variations result in oscillations in the value of arrival time step. By measuring the arrival times of white and black lines on a zebra tape (in an optical encoder) a rectangular wave can be plotted like that shown in Fig. 4. In this figure, $t_{ref}(n)$ and $t_{enc}(n)$ represent the arrival times of the reference encoder and the second encoder, respectively.

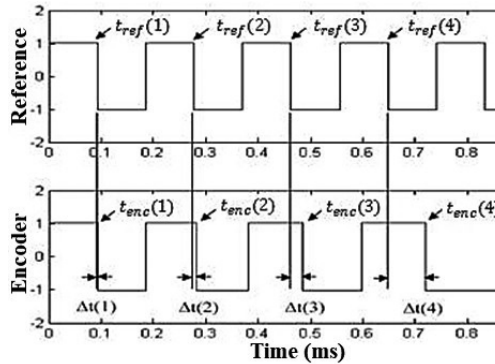


Fig. 4. Recorded signals of the encoders and the arrival times.

Using the arrival times, the time difference between passages of each two preceding divisions can be calculated as:

$$\Delta t(n) = t_{enc}(n) - t_{ref}(n), \quad (14)$$

t_{enc} and t_{ref} are the measured times of the rectangular wave shown in Fig. 4, and the torsional vibration can be calculated by using the time difference vector as:

$$\theta(n) = 360\Delta t(n)f_{shaft}, \quad (15)$$

where f_{shaft} is the angular speed of the rotor in Hz. The resulting sampling frequency in this method is:

$$f_{samp} = f_{shaft} \times N_e. \quad (16)$$

5. Results

Figure 5 shows the result of applying the method of average mutual information to the vertical vibrations at 600 rpm and 1200 rpm. The first local minimum in each figure is considered as the best time delay for reconstruction of the phase space at that speed. Fig. 6 shows the reconstructed

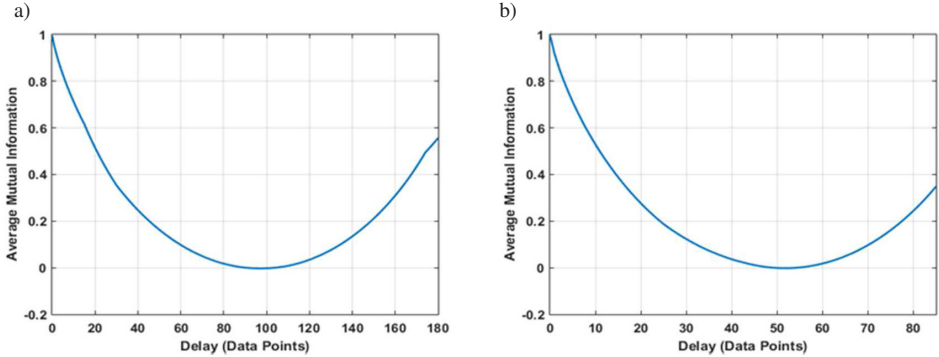


Fig. 5. Diagrams of average mutual information vs. time delay for vibrations in the vertical direction: a) 600 rpm; b) 1200 rpm.

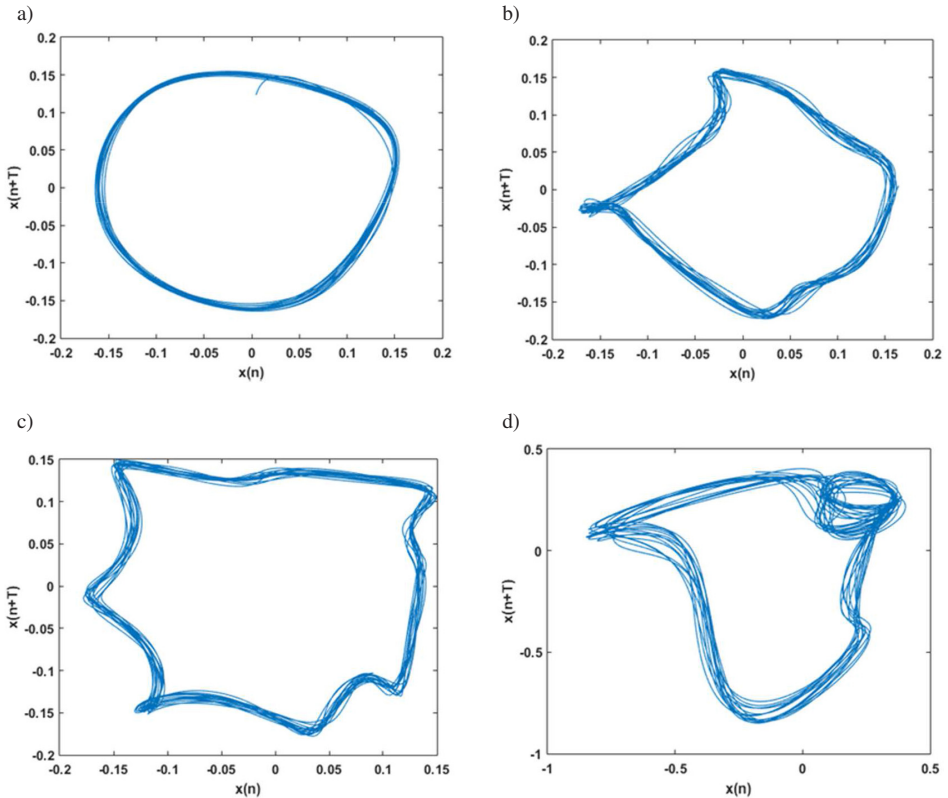


Fig. 6. Reconstructed phase planes of the system at 600 rpm: a) healthy system; b) cracked rotor; c) rotor-stator rub; d) cracked rotor with rub.

phase planes of the system for different faults at 600 rpm. In this figure, the change in the system behaviour from an almost periodic in the healthy condition to nonlinear and chaotic for a defective system is seen. This shows the nonlinear natures of the cracks and rub.

Figures 7a and 7b show the LLEs at 600 rpm and 1200 rpm, respectively. It is observed from Fig. 7 that a fault in the system increases the value of LLE of the vibration signal. The difference between the values of LLEs for the non-defective and faulty conditions are significant. The change in the value of LLE is also noticeable for most of the fault cases comparing with for the health condition. The increase in the value of LLE shows the complexity of the vibration signals that are caused by faults in the system. Another point noticed by comparing the two parts of Fig. 7 is that the calculated value of LLE for rub at 1200 rpm has a significant increase comparing with that at 600 rpm. This can be a result of higher vibration amplitudes at 1200rpm and a more severe contact between the rotor and stator, which have a constant air gap between them. Fig. 8 shows the values of correction dimension for different health conditions of the system and speeds of 600 rpm and 1200 rpm.

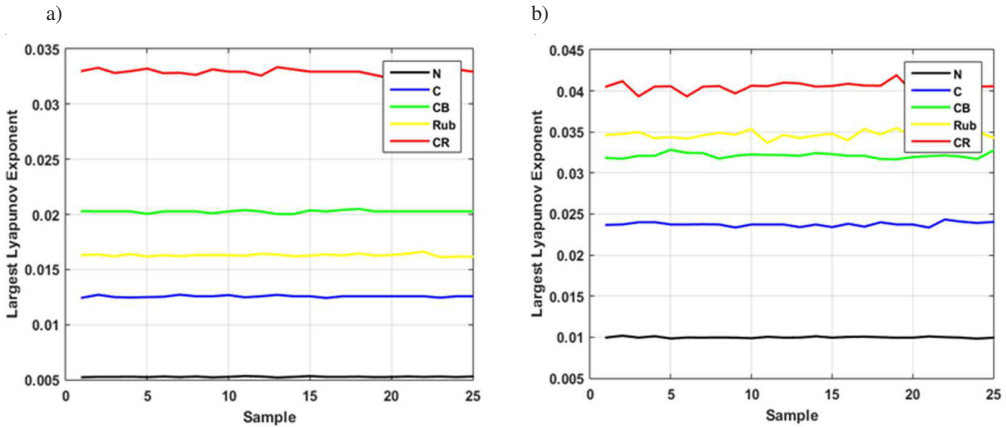


Fig. 7. The values of LLE during the tests: a) 600 rpm; b) 1200 rpm. (N and C stand for non-defective and cracked rotor, respectively. CB, Rub and CR stand for cracked rotor under radial force, intact rotor with rub and rotor with rub and crack, respectively).

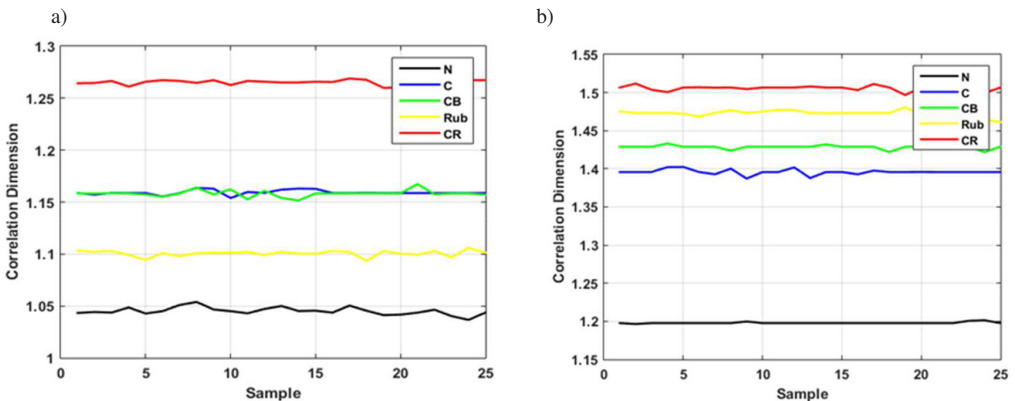


Fig. 8. The values of correlation dimension: a) 600 rpm; b) 1200 rpm.

It is observed from Fig. 8 that the calculated values of this parameter are increased for all the fault conditions comparing with that for the healthy condition. This is a result of increases in complexity and unpredictability of the vibration signal of a defected system. The difference between the curves of the healthy and defected systems is noticeable. By applying the radial force to point#6 in Fig. 1, almost the same results is obtained.

According to the equations of the previous section, it is obvious that the process of calculating ApEn depends on two parameters: the embedding dimension d and the coefficient k . Based on the references [12, 13, 15] the values of these parameters are considered as $d = 2$ and $k = 0.4$. As a result, the values of ApEn for different types of fault and different speeds are shown in Fig. 9. For ApEn, because of more frequency components and complexity of the vibration signal in a faulty system the values of ApEn are higher comparing with that in the fault-free system.

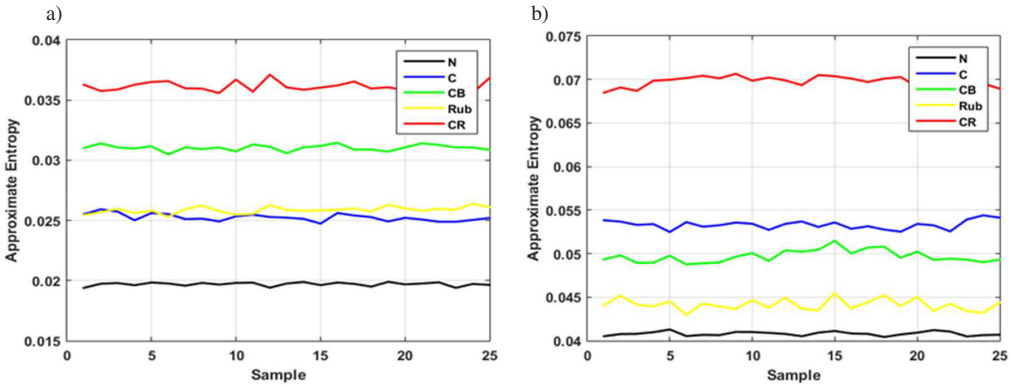


Fig. 9. The values of ApEn: a) 600 rpm; b) 1200 rpm.

After extracting the chaotic features and examining their values for different conditions, a feature space is prepared. It comprises the extracted features. This feature space is then plotted for all the faults and all the shaft speeds of 600 rpm, 900 rpm, 1200 rpm and 1500 rpm in Fig. 10. In this figure, three axes represent values of LLE, correlation dimension and ApEn, respectively. It is observed that the clusters of different fault conditions have no interference. There is also enough Euclidean distance between the centers of different clusters. Therefore, these features can be used as effective features in fault detection and diagnosis of rotors in combination with different types of vibration features or analysis techniques.

In order to evaluate the complexity of this diagnosis case and also check the effectiveness of the features, three conventional time-domain features (RMS, crest factor and kurtosis) are also extracted from the signals. These three simple statistical features, which have been used in many machinery diagnosis research studies, can be used to classify different fault conditions in low-complexity cases. Their advantage over complex features is the fast algorithm of calculation, although in many cases their values do not give a reasonable clue to the users as how to find the fault condition.

Therefore, in order to evaluate these features, first the values of each of these features are calculated for each shaft speed. These values are plotted versus sample numbers in Fig. 11 to Fig. 13. It is apparent that, unlike the chaotic features, the values of these statistical features do not change according to the changes in the health condition of the rotor. The RMS value at the normal condition varies in the same range as the RMS value for a cracked or rubbing rotor. According to Fig. 12, it is inferred that kurtosis value has a less promising pattern, where except

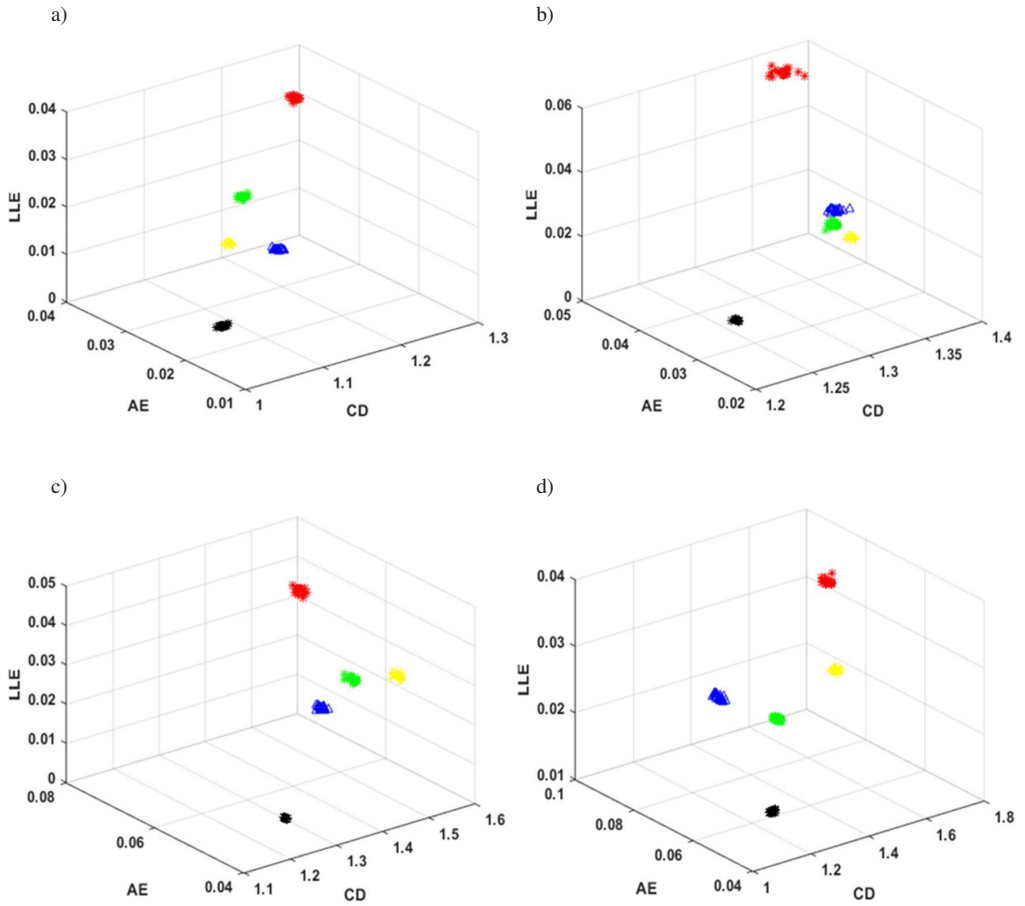


Fig. 10. Fault diagnosis in a feature space of chaotic features: a) 600 rpm; b) 900 rpm; c) 1200 rpm; d) 1500 rpm.

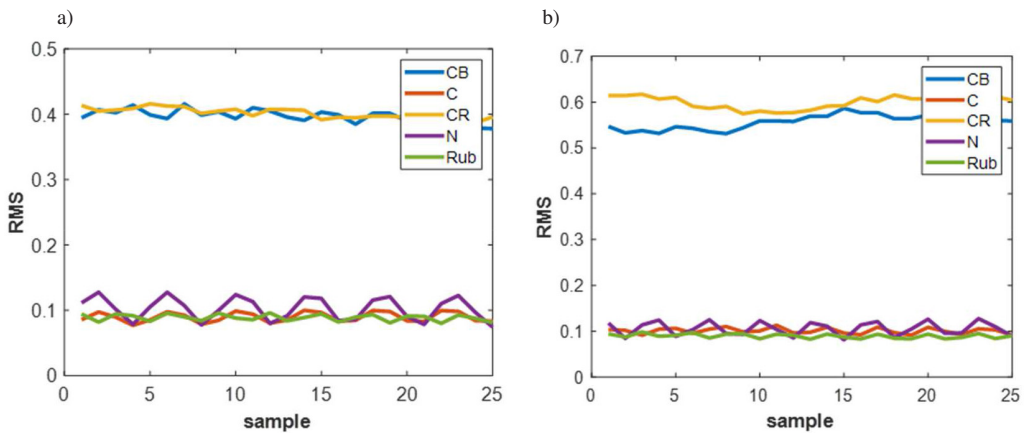


Fig. 11. The values of RMS during the tests: a) 600 rpm; b) 1200 rpm.

for its values for a rubbing rotor at 1200 rpm, the curves for other conditions intersect. Fig. 13 shows that Crest Factor is not an effective feature for fault diagnosis of this system. There is no specific level for the value of Crest Factor in each fault condition. In summary, evaluating each of these three statistical features does not give any powerful discriminating tool for fault diagnosis. Therefore, their combination has to be considered.

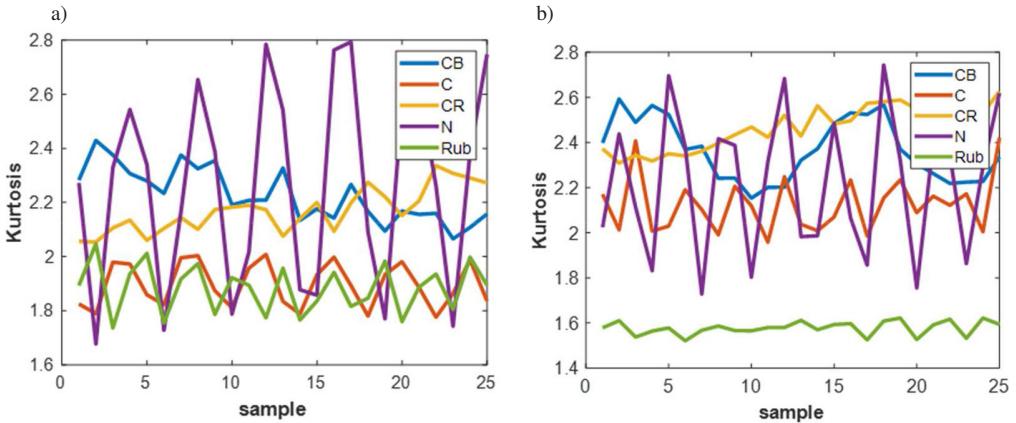


Fig. 12. The values of kurtosis: a) 600 rpm; b) 1200 rpm.

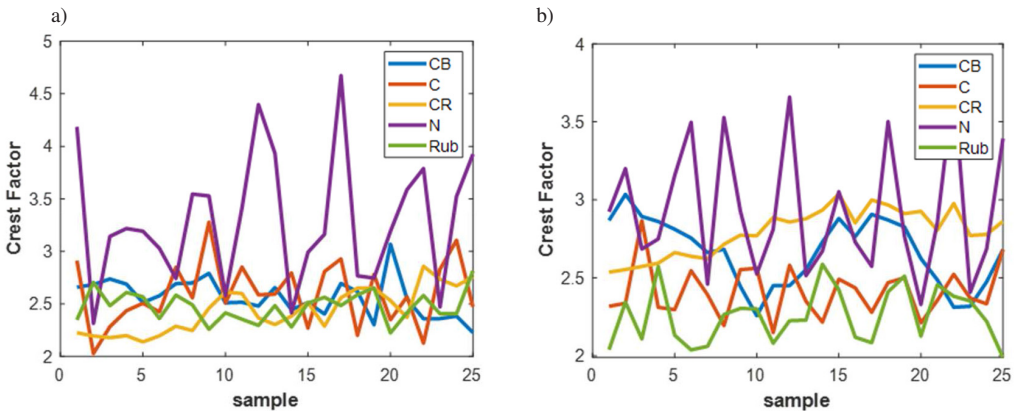


Fig. 13. The values of Crest Factor: a) 600 rpm; b) 1200 rpm.

As said before, studying the feature space determines whether a combination of features forms an effective feature set for classification of fault conditions. Therefore, the values of kurtosis, Crest Factor and RMS are assigned to three components in a 3-dimensional coordinate system. In Fig. 14, the feature spaces for four different shaft speeds are shown. Because the feature is based on the values of the features for each condition and speed, which were studied for two speeds in Fig. 11 to Fig. 13, the clusters have overlaps and most of them are not clearly separated. There are two groups of clusters. One has two clusters and the other has three. The clusters in each group are mixed. It means also that a combination of these three statistical features is not suitable for diagnosing the fault type. These feature spaces show the importance of the proposed chaotic features in classification of the five fault conditions.

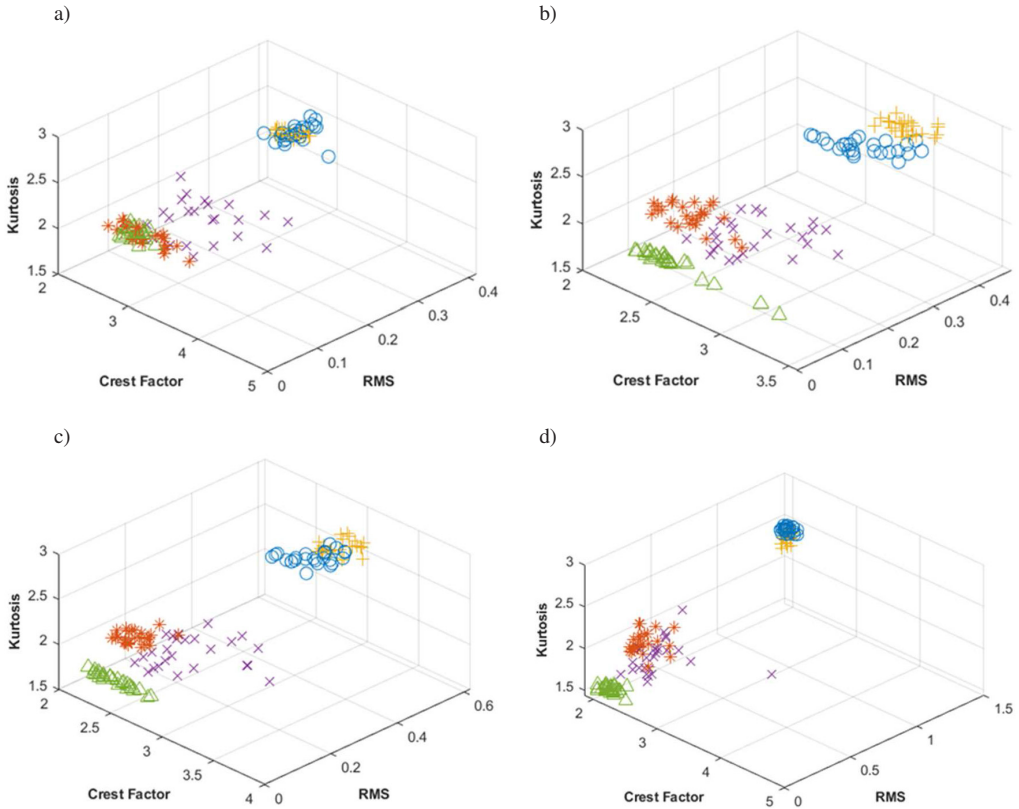


Fig. 14. Fault diagnosis in a feature space of statistical features: a) 600 rpm; b) 900 rpm; c) 1200 rpm; d) 1500 rpm.

In the next step, the same feature space is formed based on torsional vibrations. This feature space is shown for different speeds of the rotor in Fig. 11. Similar to the lateral vibrations, torsional vibrations have separate clusters in the feature space that show a potential capability of applying

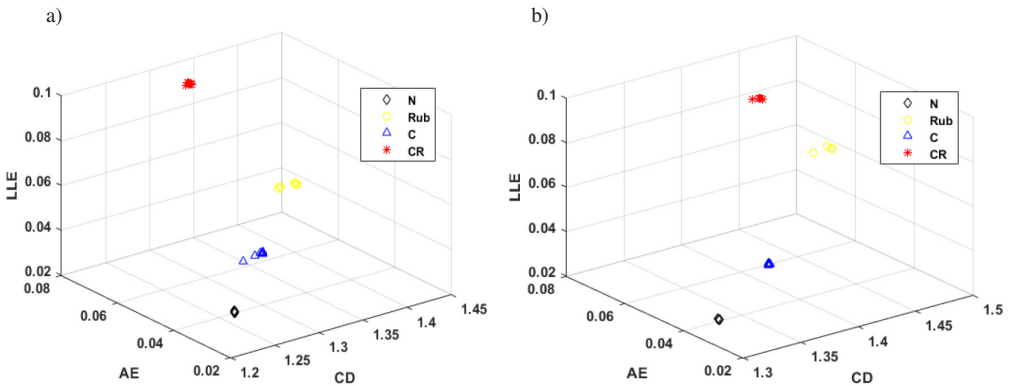


Fig. 15. Fault diagnosis in a feature space of chaotic features extracted from torsional vibrations: a) 600 rpm; b) 900 rpm; c) 1200 rpm.

these features to crack and rub detection of rotors. The normal case shows completely different values of features. It is also observed that all the fault conditions have a unique range of values for each feature. This leads to an accurate classification, which is seen as completely separated clusters with close nodes in each cluster.

In all the studied cases, the feature spaces are plotted, which show the effectiveness of the chaotic features. The clusters of fault conditions are separated if the chaotic features are used, which means an unknown condition can be identified by calculating the values of features in that condition and examining its distance to the obtained clusters. In more complicated cases with lower levels of signal to noise ratios, applying other features in addition to the chaotic ones and using an artificial neural network as a classifier increases the diagnosis accuracy. There are also feature selection algorithms, which can reduce the number of input features in order to boost the classification success and speed. All these techniques can be applied as a combination if the system faults and their symptoms are not clearly identified.

6. Conclusions

In summary, a method for examining the lateral and torsional vibrations of rotors caused by cracks or rub was proposed. A test setup was prepared and the behaviour of a rotor with cracks and rub was studied, practically. In order to measure the lateral vibrations, non-contact probes were used. Torsional vibrations were also measured by designing a measurement system based on fibre-optic sensors. The phase-space reconstruction method was used for examining the influence of the faults on the chaotic behaviour of the system. Then, the phase plane of the system was studied in each health condition of the system. The changes in the phase plane of the system in different health conditions were noticeable. ApEn, correlation dimension and LLE in each fault condition were calculated and used as chaotic features for fault diagnosis. These features showed significant changes in their values in different health condition of the system. The values of three common statistical features were also compared with the proposed chaotic features, which showed the superiority of the proposed features. By creating a feature space, the health conditions of the system for different samples were easily classified as separate clusters. Therefore, the phase plane and the introduced chaotic features can be used as classification features for fault detection and diagnosis in rotors, especially in the case of rub or cracks.

Acknowledgements

The authors would like to thank Shahid Chamran University of Ahvaz for their financial support.

References

- [1] Abadi, M.K.B., Hajnayeb, A., Hosseingholizadeh, A., Ghasemlooia, A. (2011). Single and multiple misfire detection in internal combustion engines using vold-kalman filter order-tracking. *SAE Technical Paper*.
- [2] Qin, Y. (2018). A new family of model-based impulsive wavelets and their sparse representation for rolling bearing fault diagnosis. *IEEE Transactions on Industrial Electronics*, 65, 2716–26.

- [3] Zak, G., Wylomanska, A., Zimroz, R. (2018). Local damage detection method based on distribution distances applied to time-frequency map of vibration signal. *IEEE Transactions on Industry Applications*.
- [4] Azizi, R., Attaran, B., Hajnayeb, A., Ghanbarzadeh, A., Changizian, M. (2017). Improving accuracy of cavitation severity detection in centrifugal pumps using a hybrid feature selection technique. *Measurement*, 108, 9–17.
- [5] Deng, W., Yao, R., Zhao, H., Yang, X., Li, G. (2017). A novel intelligent diagnosis method using optimal LS-SVM with improved PSO algorithm. *Soft Computing*, 1–18.
- [6] Hajnayeb, A., Ghasemloonia, A., Khadem, S., Moradi, M. (2011). Application and comparison of an ANN-based feature selection method and the genetic algorithm in gearbox fault diagnosis. *Expert Systems with Applications*, 38, 10205–10209.
- [7] Jiang, Y., Zhu, H., Li, Z. (2016). A new compound faults detection method for rolling bearings based on empirical wavelet transform and chaotic oscillator. *Chaos, Solitons & Fractals*, 89, 8–19.
- [8] Li, Z., Peng, Z. (2016). A new nonlinear blind source separation method with chaos indicators for decoupling diagnosis of hybrid failures: A marine propulsion gearbox case with a large speed variation. *Chaos, Solitons & Fractals*, 89, 27–39.
- [9] Medina, R., Alvarez, X., Jadán, D., Cerrada, M., Sánchez, R.V., Macancela, J.C. (2017). Poincaré plot features from vibration signal for gearbox fault diagnosis. *Ecuador Technical Chapters Meeting (ETCM)*, 1–6.
- [10] Wang, W., Chen, J., Wu, Z. (2000). The application of a correlation dimension in large rotating machinery fault diagnosis. *Proc. of the Institution of Mechanical Engineers, Part C: Journal of Mechanical Engineering Science*, 921–930.
- [11] Wang, W., Wu, Z., Chen, J. (2001). Fault identification in rotating machinery using the correlation dimension and bispectra. *Nonlinear Dynamics*, 25, 383–393.
- [12] Zhihong, Z., Yongqiang, L. (2012). Wheelset bearing vibration analysis based on nonlinear dynamical method. *Journal of Theoretical & Applied Information Technology*, 45.
- [13] Shuting, W., Heming, L., Zhaofeng, X. (2002). A new method of turbine-generator vibration fault diagnosis based on correlation dimension and ANN. *Power System Technology, Proc. PowerCon 2002 International Conference*, 1655–1659.
- [14] Yan, R., Gao, R.X. (2007). Approximate entropy as a diagnostic tool for machine health monitoring. *Mechanical Systems and Signal Processing*, 21, 824–839.
- [15] He, Y., Zhang, X. (2012). Approximate entropy analysis of the acoustic emission from defects in rolling element bearings. *Journal of Vibration and Acoustics*, 134, 061012.
- [16] Zhou, B., Lu, C., Li, L., Chen, Z. (2016). Health assessment for rolling bearing based on local characteristic-scale decomposition – Approximate entropy and manifold distance. *Intelligent Control and Automation (WCICA)*, 401–406.
- [17] Sadooghi, M.S., Khadem, S.E. (2018). Improving one class support vector machine novelty detection scheme using nonlinear features. *Pattern Recognition*, 83, 14–33.
- [18] Wang, L., Wang, H., Zhang, K., Zhao, W. (2007). Application of Lyapunov exponents to fault diagnosis of rolling bearing. *Noise and Vibration Control*, 5, 104–105.
- [19] Lu, C., Sun, Q., Tao, L., Liu, H., Lu, C. (2013). Bearing health assessment based on chaotic characteristics. *Shock and Vibration*, 20, 519–530.
- [20] Soleimani, A., Khadem, S. (2015). Early fault detection of rotating machinery through chaotic vibration feature extraction of experimental data sets. *Chaos, Solitons & Fractals*, 78, 61–75.

- [21] Vance, J., French, R. (1986). Measurement of torsional vibration in rotating machinery. *Journal of Mechanisms, Transmissions, and Automation in Design*, 108, 565–577.
- [22] Maynard, K.P., Trethewey, M. (1999). On the feasibility of blade crack detection through torsional vibration measurements. *Proce. of the 53 rd Meeting of the Society for Machinery Failure Prevention Technology*, Virginia Beach, 451–459.
- [23] Resor, B.R., Trethewey, M.W., Maynard, K.P. (2005). Compensation for encoder geometry and shaft speed variation in time interval torsional vibration measurement. *Journal of Sound and Vibration*, 286, 897–920.
- [24] Trethewey, M.W., Lebold, M.S., Turner, M.W. (2011). Minimally intrusive torsional vibration sensing on rotating shafts. *Structural Dynamics*, 3, 207–212.
- [25] Rosenstein, M.T., Collins, J.J., De Luca, C.J. (1993). A practical method for calculating largest Lyapunov exponents from small data sets. *Physica D: Nonlinear Phenomena*, 65, 117–134.
- [26] Grassberger, P., Procaccia, I. (1983). Measuring the strangeness of strange attractors. *Physica D: Nonlinear Phenomena*, 9, 189–208.